Physica A 451 (2016) 456–464

Contents lists available at ScienceDirect

Physica A

journal homepage: www.elsevier.com/locate/physa

The stationary non-equilibrium plasma of cosmic-ray electrons and positrons

Roman Tomaschitz

Sechsschimmelgasse 1/21-22, A-1090 Vienna, Austria

HIGHLIGHTS

- The thermodynamic variables of the cosmic-ray electron–positron plasma are calculated.
- Spectral fits to the AMS-02 and HESS GeV–TeV electron and positron fluxes are performed.
- A semi-empirical phase-space reconstruction of the partial probability densities is carried out.
- Partition function & entropy of a relativistic plasma in stationary non-equilibrium are derived.
- The positron fraction extrapolated to TeV energies shows a broad peak & exponential decay.

ARTICLE INFO

Article history:
Received 22 February 2015
Received in revised form 8 September 2015
Available online 8 February 2016

Keywords:
Stationary non-equilibrium distributions
Cosmic-ray electron–positron plasma
Relativistic statistical ensembles
Power-law densities with exponential cutoff
Nonthermal ensemble averaging
Classical & quantum partitions with extensive entropy

ABSTRACT

The statistical properties of the two-component plasma of cosmic-ray electrons and positrons measured by the AMS-02 experiment on the International Space Station and the HESS array of imaging atmospheric Cherenkov telescopes are analyzed. Stationary non-equilibrium distributions defining the relativistic electron–positron plasma are derived semi-empirically by performing spectral fits to the flux data and reconstructing the spectral number densities of the electronic and positronic components in phase space. These distributions are relativistic power-law densities with exponential cutoff, admitting an extensive entropy variable and converging to the Maxwell–Boltzmann or Fermi–Dirac distributions in the non-relativistic limit. Cosmic-ray electrons and positrons constitute a classical (low-density high-temperature) plasma due to the low fugacity in the quantized partition function. The positron fraction is assembled from the flux densities inferred from least-squares fits to the electron and positron spectra and is subjected to test by comparing with the AMS-02 flux ratio measured in the GeV interval. The calculated positron fraction extends to TeV energies, predicting a broad spectral peak at about 1 TeV followed by exponential decay.

1. Introduction

We study the statistical mechanics of the cosmic-ray electron–positron plasma, based on high-precision spectra obtained with the Alpha Magnetic Spectrometer (AMS-02) [1,2]. We demonstrate that this plasma can be treated, in close analogy to the photon gas of the cosmic microwave background radiation, as a primordial electron gas in stationary non-equilibrium. A primordial origin is also suggested by the high isotropy of the observed fluxes. Primordiality of the cosmic-ray electron–positron plasma is tantamount to the material realization of a universal cosmic reference frame as the rest frame of a relativistic gas of massive particles. An alternative approach is to use relativistic kinetic theory, but to arrive at

E-mail address: tom@geminga.org.

http://dx.doi.org/10.1016/j.physa.2016.01.091
0378-4371/

quantitative densities suitable for spectral fitting, one has to specify production mechanisms and interaction processes with cosmic matter and radiation fields which are uncertain [3].

We perform spectral fits to the AMS-02 electron and positron fluxes and reconstruct, from the inferred spectral densities, the distribution functions of the electronic and positronic plasma components. The partial number densities are relativistic non-equilibrium distributions, exponentially cut power-law densities [4,5] which converge to the Maxwell–Boltzmann distribution for low particle velocities, the Coulomb interaction being negligible. We calculate the classical partition function, by ensemble averaging in phase space, and the entropy function which is an extensive variable. We then quantize the grand partition function and show, based on the fugacity obtained from the spectral fits, that the classical limit is realized. Finally we calculate the positron fraction and give estimates of the thermodynamic parameters of this low-density high-temperature plasma.

In Section 2, we consider a relativistic plasma in stationary non-equilibrium and relate the classical spectral number density to the empirical flux density obtained from spectral fits to the measured electron and positron fluxes (performed in Section 5). In Section 3, we derive the thermodynamic variables of the electronic and positronic plasma components in phase space, based on probability distributions inferred from the spectral fits, in particular the electronic/positronic energy and entropy densities.

In Section 4, we explain the quantization of the classical nonthermal partition function and demonstrate that the classical limit applies to the cosmic-ray electron–positron plasma due to the small fugacity. The formalism developed in Sections 2–4 is based on relativistic dispersion relations and designed to be practically suitable for spectral fits in any energy range. Foundational aspects of relativistic statistical mechanics and thermodynamics such as the arrow of time and entropy are discussed in Refs. [6–9]. Recent applications of relativistic statistical mechanics include the quark–gluon plasma [10,11], plasmas in gravitational fields [12], gases of neutral particles with long-range spin–spin interaction [13] and condensation effects in relativistic Bose–Einstein gases [14]. Kinetic theory with relativistic dispersion relations, in particular the relativistic Boltzmann equation in Grad's moment expansion and Chapman–Enskog approximation, is discussed in Refs. [15,16] and a relativistic version of the Fokker–Planck equation in Ref. [17].

In Section 5, we perform least-squares fits to the AMS-02 and HESS [18] electron and positron spectra. The measured spectra are located in the GeV and low TeV range, where we can use the ultra-relativistic approximation of the spectral densities derived in Sections 2–4, which means to drop the mass term in the electronic dispersion relation. The ultra-relativistic electronic/positronic flux densities obtained in this way are then used to assemble the positron fraction, which has been measured by the AMS-02 Collaboration in the GeV range [19], thus providing a test of the spectral number densities on which the thermodynamic variables are based. Extrapolation of the analytic formula for the positron fraction into the TeV range suggests an extended spectral peak centered around 1 TeV and exponential decay above 10 TeV.

As mentioned, this primordial approach to the cosmic-ray electron–positron plasma is alternative to the use of kinetic equations which require the assumption of specific electron/positron production mechanisms [20]. A possible mechanism is electron/positron emission caused by interaction of high-energy protons or heavier cosmic-ray nuclei with the interstellar medium [3,21]. Quantitative models thereof turn out to be inconsistent with the pronounced rise of the positron fraction, so that additional positron sources have to be invoked, for instance, discrete high-energy sources such as pulsar magnetospheres or the shocked plasmas of supernova remnants [22], even if isotropy is somewhat compromised. Other authors prefer positron production via decay or annihilation of a variety of hypothetical dark matter particles at TeV energies [23] which could exist in galactic halos.

In Section 5, we also give estimates of the specific energy and number densities, entropy production, temperature, fugacity and chemical potential of the electronic/positronic plasma components. We calculate the specific densities of the actually measured electrons/positrons in the energy range above 1 GeV up to low TeV energies where an exponential cutoff occurs. We then restore the electron mass in the dispersion relation and extrapolate the analytic spectral densities obtained from the spectral fits to lower energies. In this way, we can predict the specific energy, number and entropy densities of the complete statistical ensemble comprising all gas particles by integrating the electronic/positronic spectral densities down to the electron mass. In Section 6, we present our conclusions.

2. Relativistic plasma in stationary non-equilibrium

We start with the classical number density of a free electron plasma,

$$\frac{\mathrm{d}\rho_{\mathrm{B}}}{\mathrm{d}E} = \frac{s}{2\pi^2}E^2\mathrm{e}^{-\beta E - f(E) - \alpha}\sqrt{1-m^2/E^2}, \tag{2.1}$$

$\hbar = c = 1$, where m is the electron mass, s the spin multiplicity, $\mathrm{e}^{-\alpha}$ the fugacity and $\beta = 1/(k_{\mathrm{B}}T)$ the temperature parameter. $f(E)$ is an empirical spectral function with logarithmic energy dependence, which we parametrize as $f(E) = -\log(g(E)/g(m))$, where $g(E)$ is a positive but otherwise arbitrary function obtained from a spectral fit. The normalization with $g(m)$ means $f(m) = 0$, and the classical Maxwell–Boltzmann (or Jüttner) equilibrium distribution of a free relativistic electron gas is recovered in the limit of vanishing $f(E)$, see Ref. [9] and references therein.

The number density (2.1) is assembled with the integration measure $s\mathrm{d}^3p/(2\pi)^3$ and the dispersion relation for free relativistic particles $p = \sqrt{E^2-m^2}$, so that $\mathrm{d}^3p = 4\pi\sqrt{1-m^2/E^2}E^2\mathrm{d}E$. The normalization factor $s/(2\pi)^3$ arises from

box quantization in the continuum limit, see (4.4). The quantized spectral density of which (2.1) is the classical limit is discussed in Section 4. Density (2.1) is thus assembled as $\mathrm{d}\rho_{\mathrm{B}} = (2\pi)^{-3} s G(E) \mathrm{e}^{-\beta E-\alpha} \mathrm{d}^3p$, with the normalized spectral function $G(E) = g(E)/g(m)$. The non-relativistic limit of $\mathrm{d}\rho_{\mathrm{B}}(E)$ is thermal since $g(E) = g(m) + \mathrm{O}(\upsilon^2)$, $E = m/\sqrt{1-\upsilon^2}$, where $\upsilon \ll 1$ is the particle speed parametrizing the non-relativistic Maxwell–Boltzmann distribution, whose chemical potential is obtained from the relativistic potential μ [GeV] $= -\alpha/\beta$ by subtraction of the rest mass m.

The spectral flux density is found by multiplying the number density with the group velocity, $\upsilon = \mathrm{d}E/\mathrm{d}p = \sqrt{1-m^2/E^2}$. The flux density per steradian is thus

$$\Phi_E \ [\mathrm{GeV}^{-1}\ \mathrm{sr}^{-1}\ \mathrm{m}^{-2}\ \mathrm{s}^{-1}] = \frac{1}{4\pi}\sqrt{1-\frac{m^2}{E^2}}\,\frac{\mathrm{d}\rho_{\mathrm{B}}}{\mathrm{d}E}, \tag{2.2}$$

where we have indicated the units used in the spectral fits. We rescale with E^3 to find

$$E^3\Phi_E \ [\mathrm{GeV}^{2}\ \mathrm{sr}^{-1}\ \mathrm{m}^{-2}\ \mathrm{s}^{-1}] = \frac{s}{8\pi^3}E^5\frac{g(E)}{g(m)}\mathrm{e}^{-\beta E-\alpha}\left(1-\frac{m^2}{E^2}\right). \tag{2.3}$$

The spectral fits in Section 5 are performed with the flux density [24,25]

$$E^3\Phi_E = A_\Phi E^{\alpha_1}\frac{1+(E/c_1)^{\gamma_1}}{1+(E/b_1)^{\beta_1}}\mathrm{e}^{-\beta E}\left(1-\frac{m^2}{E^2}\right), \tag{2.4}$$

where the exponents α_1, β_1, γ_1, β and amplitudes A_Φ, b_1, c_1 are fitting parameters. The factor $1-m^2/E^2$ stems from the electronic dispersion relation $p = E\sqrt{1-m^2/E^2}$ which enters both in the group velocity $\mathrm{d}E/\mathrm{d}p$ and the integration measure d^3p stated above. (We have put $\hbar = 1$, so that the momentum variable p of free particles coincides with their wavenumber k, cf. Section 4.) In the ultra-relativistic limit, one assumes that the mass/energy ratio is small compared to 1 so that it can be dropped, $p \sim E$. The spectral fits in Section 5 are performed in the GeV interval, the ultra-relativistic regime, where the squared ratio is smaller than 10^{-6}, so that the flux density becomes effectively independent of the electron mass at GeV energies and above. In the relativistic formalism developed in Sections 2–4, we maintain this ratio in the dispersion relation, so that the spectral densities defining the thermodynamic variables remain valid for particle energies close to the rest mass and in the intermediate regime.

In flux density (2.4), we specified the spectral function $g(E)$ in (2.3) by the ansatz

$$g(E) = E^{\alpha_1-5}\frac{1+(E/c_1)^{\gamma_1}}{1+(E/b_1)^{\beta_1}}, \tag{2.5}$$

and the flux amplitude A_Φ reads

$$A_\Phi \ [\mathrm{GeV}^{2-\alpha_1}\ \mathrm{sr}^{-1}\ \mathrm{m}^{-2}\ \mathrm{s}^{-1}] = \frac{s}{(2\pi\hbar)^3c^2}\frac{\mathrm{e}^{-\alpha}}{g(m)} \approx 3.146\times 10^{53}\frac{\mathrm{e}^{-\alpha}}{g(m)}. \tag{2.6}$$

Here, we have restored the units, put $s = 2$ (spin multiplicity), and used GeV units for the electron mass and the coefficients c_1 and b_1 in (2.5).

The number of particles in a volume V with energies exceeding $E_{\mathrm{cut}} \geq m$ is calculated as

$$N = -\frac{\partial}{\partial\alpha}\log Z_{\mathrm{B}}(\beta,\alpha,V) = V\int_{E_{\mathrm{cut}}}^{\infty}\mathrm{d}\rho_{\mathrm{B}}(E), \tag{2.7}$$

and the total energy of particles with energies above E_{cut} is

$$U = -\frac{\partial}{\partial\beta}\log Z_{\mathrm{B}}(\beta,\alpha,V) = V\int_{E_{\mathrm{cut}}}^{\infty}E\mathrm{d}\rho_{\mathrm{B}}(E). \tag{2.8}$$

In Section 5, we will use the lower edge of the measured spectrum as cutoff energy, putting $E_{\mathrm{cut}} = 1$ GeV, so that specific densities like U/V refer to the observed GeV and low-TeV electrons/positrons. We will also extrapolate the analytic spectral measure $\mathrm{d}\rho_{\mathrm{B}}(E)$ obtained from the spectral fits to lower energies and identify E_{cut} in (2.8) with the electron mass m to obtain the total specific densities covering all particle energies above the rest mass. In this case, the electronic specific energy density increases to 4.95 keV/m^3 as compared with a density of 4.17 keV/m^3 comprising electrons exceeding the experimental threshold energy of 1 GeV, see Table 2 in Section 5. (For comparison, the specific energy density of the primordial photon background is 261 keV/m^3.) In Table 2, we record the specific particle, energy and entropy densities of electrons/positrons in the measured GeV–TeV interval ($E_{\mathrm{cut}} = 1$ GeV) as well as the total specific densities based on the extrapolated spectra ($E_{\mathrm{cut}} = m$), also see the discussion at the end of Section 5.

Entropy is an extensive quantity proportional to V,

$$S(\beta,\alpha,V) = k_{\mathrm{B}}(\log Z_{\mathrm{B}} + \beta U + \alpha N), \tag{2.9}$$

where we can replace the logarithm of the classical partition function $\log Z_{\mathrm{B}}$ by the particle number N.

To demonstrate thermodynamic stability, we first show that the inequalities $0 \le C_V \le C_P$ hold for the isochoric and isobaric heat capacities. To this end, we note, cf. (2.7) and (2.8),

$$U(\beta, N) = -N\frac{\partial \log K}{\partial \beta}, \qquad K(\beta) = \int_{E_{\rm cut}}^{\infty} E^2 \mathrm{e}^{-\beta E - f(E)}\sqrt{1-m^2/E^2}\,\mathrm{d}E \tag{2.10}$$

and

$$C_V = \frac{\partial}{\partial T}U(\beta, N) = k_{\rm B}N\beta^2\frac{\partial^2 \log K}{\partial \beta^2}, \qquad C_P = C_V + k_{\rm B}N. \tag{2.11}$$

The Schwarz inequality $(K_{,\beta})^2 \le KK_{,\beta,\beta}$ implies $(\log K)_{,\beta,\beta} \ge 0$ (subscript commas indicate differentiation with respect to β), so that the above inequalities hold.

We also have to show mechanical stability, $0 \le \kappa_S \le \kappa_T$, where κ_S and κ_T denote adiabatic and isothermal compressibility. Since $N = \log Z_{\rm B}$, cf. (2.7), the thermal equation of state reads $P = N/(\beta V)$, and the isothermal compressibility is thus $\kappa_T = -(1/V)\partial V(\beta, P, N)/\partial P = 1/P$. The adiabatic compressibility is related to the heat capacities by $\kappa_S = \kappa_T C_V/C_P$, which implies the stated inequalities since $\kappa_T > 0$ and $C_P > C_V$. This holds true for the electronic and positronic plasma components alike.

3. Thermodynamic variables in phase space

We consider the phase space of n electrons with measure

$$\mathrm{d}^{3n}(p, q) = \frac{1}{(2\pi)^{3n}}\mathrm{d}^3p_1\mathrm{d}^3q_1\mathrm{d}^3p_2\mathrm{d}^3q_2\cdots\mathrm{d}^3p_n\mathrm{d}^3q_n,$$
$$\mathrm{d}^3p_k = 4\pi\sqrt{1-m^2/E_k^2}E_k^2\mathrm{d}E_k, \tag{3.1}$$

$k = 1, \ldots, n$. The d^3q_k integrations range over a volume V, and the $\mathrm{d}E_k$ integrations refer to the interval $E_{\rm cut} \le E_k \le \infty$, cf. (2.7) and after (2.1). The normalization $(2\pi)^{3n}$ is suggested by the quantized spectral number density (4.7) in the classical limit. The n-particle probability distribution reads

$$P_n(p, q) = \frac{s^n}{n!}b_n(p, q)h_n(p, q),$$
$$b_n = \exp\left(-\xi - \beta\sum_{k=1}^{n}E_k - \alpha n\right), \qquad h_n = \exp\left(-\sum_{k=1}^{n}f(E_k)\right). \tag{3.2}$$

The factorial accounts for indistinguishability, s is the spin degeneracy and ξ a normalization constant. The number densities listed in Table 2 are very low and the temperature of the electronic/positronic components is sufficiently high to neglect the Coulomb interaction; also see Section 6 for a numerical estimate. Otherwise we would have to incorporate the Coulomb potential in the probability density and use, for instance, the Debye–Hückel approximation to calculate the thermodynamic variables [26].

The phase-space probability is normalized to one,

$$\int\sum_{n=0}^{\infty}P_n(p, q)\mathrm{d}^{3n}(p, q) = 1, \tag{3.3}$$

where summation and integration can be interchanged and the integrals factorize. This normalization is achieved by identifying ξ in (3.2) with the logarithm of the partition function $\log Z_{\rm B} = N$, cf. (2.7). Thus,

$$Z_{\rm B} = \sum_{n=0}^{\infty}\frac{s^n}{n!}\int\exp\left(-\beta\sum_{k=1}^{n}E_k - \alpha n\right)h_n(p, q)\mathrm{d}^{3n}(p, q). \tag{3.4}$$

The expectation values of particle number and internal energy read

$$\sum_{n=0}^{\infty}\int nP_n(p, q)\mathrm{d}^{3n}(p, q) = -\frac{\mathrm{d}\xi}{\mathrm{d}\alpha} = N, \tag{3.5}$$

$$\sum_{n=0}^{\infty}\int\left(\sum_{k=1}^{n}E_k\right)P_n(p, q)\mathrm{d}^{3n}(p, q) = -\frac{\mathrm{d}\xi}{\mathrm{d}\beta} = U. \tag{3.6}$$

The spectral number density (2.1) is identified by way of (3.5). The entropy stated in (2.9) is assembled in phase space as

$$S = -k_{\rm B}\int\sum_{n=0}^{\infty}\frac{s^n}{n!}h_n(p,q)b_n(p,q)\log b_n(p,q)\mathrm{d}^{3n}(p,q), \tag{3.7}$$

which can be written as expectation value,

$$S = k_{\rm B}\int\sum_{n=0}^{\infty}\left(\xi+\beta\sum_{k=1}^{n}E_k+\alpha n\right)P_n(p,q)\mathrm{d}^{3n}(p,q). \tag{3.8}$$

4. Quantized partition function of the electronic and positronic plasma components

The quantized version of the classical partition function $Z_{\rm B}$ in (2.7) is obtained by a trace calculation in fermionic occupation number representation [25,27],

$$Z_{\rm F} = \mathrm{Tr}[\exp(-\alpha\hat{N}-\beta\hat{H}-f(\hat{H}))]. \tag{4.1}$$

The particle number operator is $\hat{N}=\sum_{|\mathbf{k}|\geq k_{\rm cut}}\hat{N}_{\mathbf{k}}$, $\hat{N}_{\mathbf{k}}=b_{\mathbf{k}}^{+}b_{\mathbf{k}}$, where the $b_{\mathbf{k}}^{(+)}$ are fermionic creation/annihilation operators. The energy operator reads $\hat{H}=\sum_{|\mathbf{k}|\geq k_{\rm cut}}E_{\mathbf{k}}\hat{N}_{\mathbf{k}}$ and the empirical spectral function $f(E)$ in (2.1) defining the deviation from equilibrium is quantized as $f(\hat{H})=\sum_{|\mathbf{k}|\geq k_{\rm cut}}f(E_{\mathbf{k}})\hat{N}_{\mathbf{k}}$. The Hermitian number operators are diagonal, $\hat{N}_{\mathbf{k}}|n\rangle=n_{\mathbf{k}}|n\rangle$, and the fermionic occupation numbers $n_{\mathbf{k}}$ attached to a wave vector $\mathbf{k}$ can take the values zero and one. Electron energy and wavenumber $k=p$ ($\hbar=c=1$) are related by the dispersion relation $E_{\mathbf{k}}=\sqrt{k^2+m^2}$, cf. after (2.4). The wavenumber of the lower energy threshold in (2.7) and (2.8) is $k_{\rm cut}=m\sqrt{E_{\rm cut}^2/m^2-1}$. We will employ box quantization, discretizing the wave vectors as $\mathbf{k}=2\pi\mathbf{n}/L$, so that $\mathbf{k}$ summations are taken over integer lattice points $\mathbf{n}$, corresponding to periodic boundary conditions on a box of size $V=L^3$.

With these prerequisites, trace (4.1) can be evaluated as

$$\begin{aligned}Z_{\rm F} &= \sum_{n_{\mathbf{k}}=0,1}\exp\sum_{|\mathbf{k}|\geq k_{\rm cut}}(-\alpha-\beta E_{\mathbf{k}}-f(E_{\mathbf{k}}))n_{\mathbf{k}}\\ &= \prod_{|\mathbf{k}|\geq k_{\rm cut}}[1+\exp(-\alpha-\beta E_{\mathbf{k}}-f(E_{\mathbf{k}}))].\end{aligned} \tag{4.2}$$

By taking the logarithm, we find

$$\log Z_{\rm F} = \sum_{|\mathbf{k}|\geq k_{\rm cut}}\log(1+\mathrm{e}^{-\alpha-\beta E_{\mathbf{k}}-f(E_{\mathbf{k}})}). \tag{4.3}$$

Performing the continuum limit $L\to\infty$ and taking into account the spin degeneracy, we can replace the summation in (4.3) by the integration $sV\int_{|\mathbf{k}|\geq k_{\rm cut}}\mathrm{d}^3k/(2\pi)^3$,

$$\log Z_{\rm F} = \frac{sV}{(2\pi)^3}\int_{|\mathbf{k}|\geq k_{\rm cut}}\log(1+\mathrm{e}^{-\alpha-\beta E_{\mathbf{k}}-f(E_{\mathbf{k}})})\mathrm{d}^3k. \tag{4.4}$$

The integration measure d^3k is parametrized like d^3p indicated after (2.1),

$$\log Z_{\rm F} = \frac{Vs}{2\pi^2}\int_{E_{\rm cut}}\log(1+\mathrm{e}^{-\alpha-\beta E-f(E)})\sqrt{1-m^2/E^2}E^2\mathrm{d}E. \tag{4.5}$$

The quantized spectral number density $\mathrm{d}\rho_{\rm F}(E)$ is identified by means of the particle number,

$$N = -\frac{\partial}{\partial\alpha}\log Z_{\rm F} = V\int_{E_{\rm cut}}^{\infty}\mathrm{d}\rho_{\rm F}(E), \tag{4.6}$$

$$\mathrm{d}\rho_{\rm F}(E) = \frac{s}{2\pi^2(\hbar c)^3}\frac{\sqrt{1-m^2/E^2}}{\mathrm{e}^{\alpha+\beta E+f(E)}+1}E^2\mathrm{d}E. \tag{4.7}$$

The nonthermal Fermi density (4.7) can be replaced by the Boltzmann density $\mathrm{d}\rho_{\rm B}(E)$ in (2.1) if $\mathrm{e}^{\alpha+\beta E+f(E)}\gg 1$. As the inverse fugacity $\mathrm{e}^{\alpha}=1/z$ turns out to be very large, cf. Table 2, we can use the classical limit (2.1) to calculate the thermodynamic parameters of the electronic and positronic components, cf. (5.3).

Table 1
Fitting parameters of the electronic (e^-) and positronic (e^+) flux densities. The spectral fits depicted in Figs. 1 and 2 are performed with the ultra-relativistic flux density $E^3\Phi_E \sim A_\Phi E^{\alpha_1}\frac{1+(E/c_1)^{\gamma_1}}{1+(E/b_1)^{\beta_1}}e^{-\beta E}$, cf. (2.4) and (5.1). Listed are the flux amplitude A_Φ, the power-law exponents $\alpha_1, \beta_1, \gamma_1$, the power-law amplitudes b_1, c_1, and the temperature parameter β in the exponential. Derived thermodynamic parameters of the electronic/positronic plasma components are recorded in Table 2.

	A_Φ (GeV$^{2-\alpha_1}$ sr^{-1} m^{-2} s^{-1})	α_1	b_1 (GeV)	β_1	c_1 (GeV)	γ_1	$\beta \times 10^3$ (GeV^{-1})
e^-	21.34 ± 0.617	2.134 ± 0.050	3.584 ± 0.119	2.453 ± 0.035	329.1 ± 62.80	1.074 ± 0.131	1.127 ± 0.137
e^+	1.966 ± 0.102	2.081 ± 0.144	2.524 ± 0.227	2.272 ± 0.080	51.30 ± 30.35	0.881 ± 0.044	1.200 ± 0.107

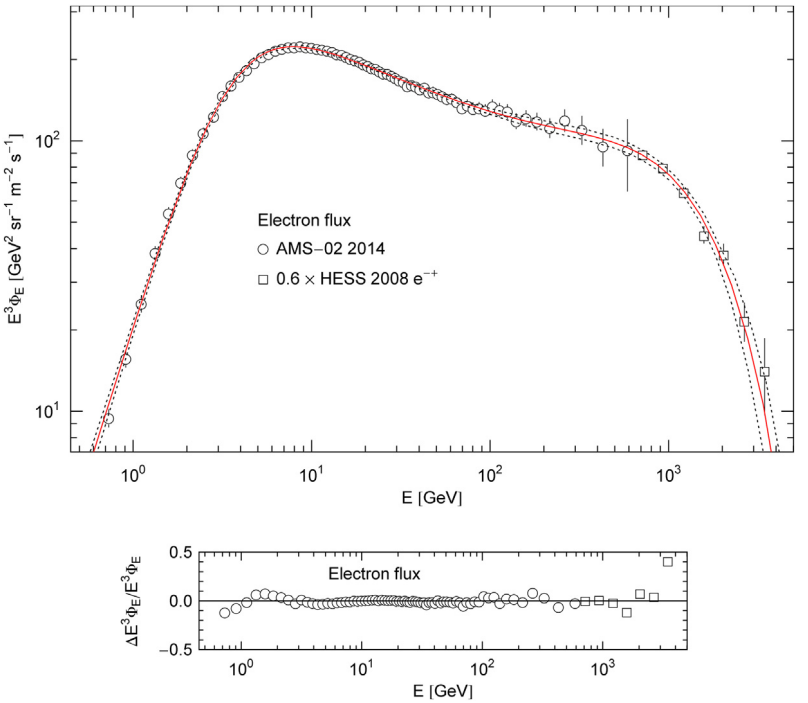

Fig. 1. Flux density of cosmic-ray electrons. Data points from AMS-02 [1] (open circles) and HESS [18] (open squares). The HESS points refer to the combined electron and positron flux and are rescaled by a factor of 0.6 to obtain a continuous transition to the AMS-02 electron flux. The solid curve is a fit of the ultra-relativistic electronic flux density $E^3\Phi_E(e^-)$ in (5.1), the fitting parameters are listed in Table 1. The error band defined by the dotted curves indicates the 2σ (95%) confidence limits of the least-squares fit, $\chi^2(e^-)/\text{dof} \approx 21.0/72$. The residuals are depicted in the lower panel. The thermodynamic parameters of the electronic and positronic plasma components are recorded in Table 2.

5. Spectral fits to high-energy cosmic-ray electron and positron fluxes

The spectral fits in Figs. 1 and 2 are performed in the GeV and TeV range, the ultra-relativistic regime, so that we can drop the factor $(1 - m^2/E^2)$ in the flux density, see the discussion following Eq. (2.4),

$$E^3\Phi_E\ [\text{GeV}^2\ \text{m}^{-2}\ \text{sr}^{-1}\ \text{s}^{-1}] \sim A_\Phi E^{\alpha_1}\frac{1+(E/c_1)^{\gamma_1}}{1+(E/b_1)^{\beta_1}}e^{-\beta E}. \tag{5.1}$$

The fitting parameters are the power-law exponents $\alpha_1, \beta_1, \gamma_1$ and amplitudes A_Φ, b_1, c_1 as well as the temperature parameter β determining the exponential cutoff; they are listed separately for the electronic and positronic plasma components in Table 1. Even though the spectral maps in Figs. 1 and 2 look quite different at first sight, they can both be reproduced with flux density (5.1). In Fig. 3, we compare the analytic flux ratio $\Phi_E(e^+)/(\Phi_E(e^-) + \Phi_E(e^+))$ obtained from the spectral fits to the measured positron fraction. We also depict the asymptotic limit of this ratio, $\sim 0.52E^{-0.066}e^{-7.4\times10^{-5}E}$ (E in GeV units), which exhibits exponential decay since the positron flux decays faster than the electron flux, cf. Table 1. The spectral fits in Figs. 1 and 2 are based on the AMS-02 and HESS 2008 flux points [1,18]. There have been several other experiments attempting to measure the cosmic-ray electron and positron fluxes above 1 GeV and the positron fraction [28–32]. They are not included in the least-squares fits, as they define different spectral curves which are only marginally compatible with the AMS-02 data sets which admit smaller error bars and extend to higher energies [1].

The classical spectral number density reads, cf. (2.1) and Refs. [33,34],

$$\text{d}\rho_{\text{B}}(E)\ [\text{m}^{-3}] \sim \frac{s}{2\pi^2(\hbar c)^3}\frac{g(E)}{g(m)}E^2e^{-\beta E-\alpha}\sqrt{1-\frac{m^2}{E^2}}\text{d}E, \tag{5.2}$$

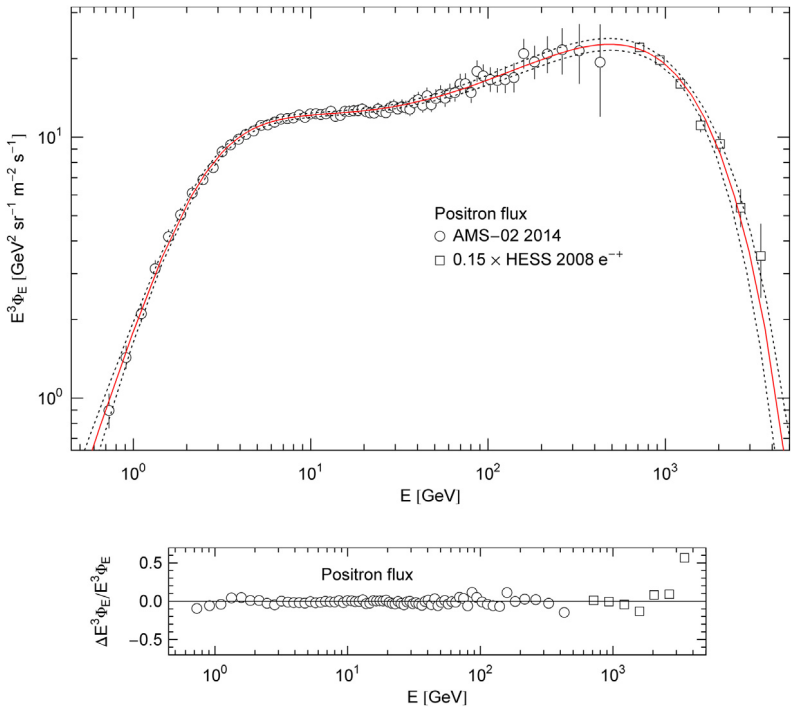

Fig. 2. Spectral flux density of the positronic plasma component. Data points from AMS-02 [1] (open circles) and HESS [18] (open squares). The caption to Fig. 1 applies. HESS flux points are rescaled by a factor of 0.15. The χ^2 fit (solid curve, $\chi^2(e^+)/\text{dof} \approx 27.2/72$) is based on the spectral flux density $E^3\Phi_E(e^+)$ in (5.1); the fitting parameters are listed in Table 1. The dotted curves depict the 2σ confidence limits, the residuals are shown in the lower panel. The highest energy HESS data point lies outside the error band, suggesting the possibility of a subexponential Weibull-type spectral decay [37–40], but this hinges on one flux point with large error bar. Preliminary estimates of the combined electron–positron flux in the low TeV region obtained with the PAMELA calorimeter [41] also indicate an exponential cutoff as depicted in Figs. 1 and 2.

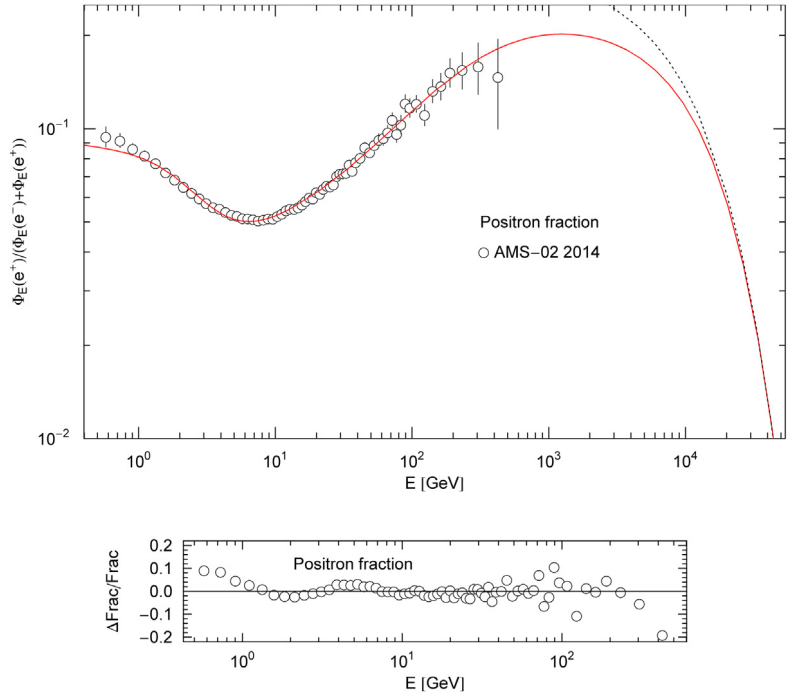

Fig. 3. Positron fraction of the cosmic-ray electron–positron plasma. Depicted is the flux ratio $\Phi_E(e^+)/(\Phi_E(e^-) + \Phi_E(e^+))$ (solid curve). The electronic/positronic flux densities $\Phi_E(e^-)$ and $\Phi_E(e^+)$ are stated in (5.1) with parameters in Table 1 (obtained from the χ^2 fits in Figs. 1 and 2). The data points (open circles) show the AMS-02 positron fraction [19]. The dotted curve is the exponentially decaying asymptotic limit of the positron fraction, see after (5.1). The residuals are plotted in the lower panel.

Table 2
Thermodynamic parameters of the cosmic-ray electron–positron plasma, cf. (5.2) and Table 1. $\hat{n}$ is the specific number density and $\hat{u}$ the specific energy density of the electronic/positronic component, cf. (5.3). Also recorded are temperature T, fugacity z, chemical potential μ and the specific entropy density $\hat{s}$; the entropy production mainly stems from the fugacity term $\alpha\hat{n}$ in (5.4) ($\alpha = -\log z$). The specific densities $\hat{n}$, $\hat{u}$ and $\hat{s}$ are listed for two lower threshold energies $E_{\rm cut}$ of the electron/positron spectrum. The cutoff energy of 1 GeV (1st and 3rd row) refers to specific densities comprising GeV and low-TeV electrons/positrons as measured by the AMS-02 spectrometer and the HESS Cherenkov array. The spectral densities (5.2) obtained from the fits in Figs. 1 and 2 can be extrapolated to lower energies; in the 2nd and 4th row, we identify $E_{\rm cut}$ with the electron mass and list the total specific densities, cf. after (5.4).

	$E_{\rm cut}$ (GeV)	$\hat{n}$ (m^{-3})	$\hat{u}$ (GeV m^{-3})	$k_{\rm B}T$ (GeV)	$\log z$	μ (GeV)	$\hat{s}/k_{\rm B}$ (m^{-3})
e^-	1	1.30×10^{-6}	4.17×10^{-6}	888	−98.4	-8.73×10^{4}	1.30×10^{-4}
e^-	0.511×10^{-3}	5.43×10^{-6}	4.95×10^{-6}	888	−98.4	-8.73×10^{4}	5.40×10^{-4}
e^+	1	9.15×10^{-8}	2.75×10^{-7}	833	−100	-8.36×10^{4}	9.28×10^{-6}
e^+	0.511×10^{-3}	5.43×10^{-7}	3.50×10^{-7}	833	−100	-8.36×10^{4}	5.51×10^{-5}

where $g(E;\alpha_1,\beta_1,\gamma_1,b_1,c_1)$ denotes the spectral function (2.5); the indicated parameters are obtained from the χ^2 fits of the electron and positron fluxes and are listed in Table 1, as are temperature $k_{\rm B}T$ [GeV] $= 1/\beta$ and fugacity $z = {\rm e}^{-\alpha}$, the latter is extracted from the flux amplitude A_Φ, cf. (2.6). We denote specific thermodynamic densities by lower case letters with a hat; the specific number and energy densities read, cf. (2.7) and (2.8),

$$\hat{n}\,[{\rm m}^{-3}] \sim \int_{E_{\rm cut}}^{\infty} {\rm d}\rho_{\rm B}(E), \qquad \hat{u}\,[{\rm GeV/m}^3] \sim \int_{E_{\rm cut}}^{\infty} E{\rm d}\rho_{\rm B}(E), \tag{5.3}$$

where ${\rm d}\rho_{\rm B}(E)$ is the relativistic spectral density (5.2). The specific entropy density $\hat{s} = S/V$ rescaled with the Boltzmann constant is assembled as, cf. (2.9),

$$\frac{\hat{s}}{k_{\rm B}}\,[{\rm m}^{-3}] = (1+\alpha)\hat{n} + \beta\hat{u}. \tag{5.4}$$

The specific particle, energy and entropy densities of the electronic and positronic plasma components are recorded in Table 2, together with temperature, fugacity and chemical potential. We list the specific densities of the observed GeV–TeV electrons and positrons and also give estimates of the total specific densities covering the complete spectrum by extrapolating the spectral measure (5.2) to lower energies and identifying the cutoff energy in (5.3) with the electron mass, $E_{\rm cut} = m$. That is, the specific densities listed in the first and third row of Table 2 comprise electrons/positrons measured by the AMS-02 experiment in the energy interval of 1 GeV up to a few TeV where the spectral densities are exponentially cut; the lower integration boundary in (5.3) is thus $E_{\rm cut} = 1$ GeV. The specific densities listed in the second and fourth row of Table 2 are also based on the analytic relativistic spectral densities (5.2) derived from the same spectral fits, but in this case we use the electron mass 0.51 MeV as lower integration boundary in (5.3), so that the densities take account of all gas particles including those in the MeV interval which cannot be resolved with the AMS-02 spectrometer. The specific densities of internal energy, number count and entropy of the positronic plasma component are by one order lower than the electronic counterparts, whereas the estimates of temperature and chemical potential are quite comparable. This holds true for the observed densities (row 1 and 3 of Table 2) as well as for the predicted densities of the total electronic/positronic plasma components recorded in row 2 and 4.

6. Conclusion

We developed a statistical description of the cosmic-ray electron–positron plasma based on stationary non-equilibrium distributions. The latter are inferred from spectral fits to the electron and positron spectra measured by the AMS-02 experiment in the GeV interval and the Cherenkov telescope HESS in the low TeV range. In particular, we do not need to make hypothetical assumptions on sources and production mechanisms of high-energy cosmic-ray electrons/positrons. Their spectral number densities are semi-empirically reconstructed from the measured electron and positron fluxes as classical ensemble averages in phase space.

The cosmic-ray electron–positron plasma is relativistic and nonthermal, the Coulomb interaction can be neglected due to the low particle density and high temperature. The criterion for this approximation is a small ratio $e^2/(4\pi d k_{\rm B}T) \ll 1$, where $d = \hat{n}^{-1/3}$ is the interparticle distance and $e^2/(4\pi) \approx 1/137$ the fine-structure constant [35,36]. In the case of cosmic-ray electrons and positrons, this ratio is of order 10^{-23}. Temperature and the specific number density $\hat{n}$ of the non-equilibrated plasma components are listed in Table 2. Quantum corrections to the classical partition function are also negligible, cf. after (4.7).

The entropy of the cosmic-ray electron–positron plasma is an extensive quantity, even though the underlying electronic/positronic probability distributions are nonthermal. We also checked the positivity of the heat capacities and compressibility, which ensures the thermodynamic stability of each plasma component implying positive root mean squares of the thermodynamic variables. The thermal Maxwell–Boltzmann distribution is recovered in the non-relativistic limit of the spectral number density (2.1).

To summarize the approximations, cosmic-ray electrons and positrons at GeV energies and beyond constitute a relativistic gas, so that one has to use relativistic dispersion relations. As the particles are charged, they constitute a two-component plasma, but since the gas is dilute and thus the interparticle distances large according to the number densities in Table 2, one can ignore Coulomb interaction and Debye screening, see the estimate above. As the fugacity is low, the quantum distribution (4.7) can be approximated by its classical limit. In the spectral fits in Section 5, the ultra-relativistic approximation is used, because the electronic mass/energy ratio is negligible in the GeV band, cf. after (2.4). In the calculation of the specific thermodynamic densities of the electronic and positronic gas components, cf. Table 2, we restored this ratio in the electronic dispersion relation, since the fitted spectral densities determining the specific densities are extrapolated to lower energies, see the remarks after (5.4).

We calculated the positron fraction using the parameters obtained from the spectral fits in Figs. 1 and 2, and compared it with the AMS-02 fraction measured in the GeV range. As the analytic representation (5.1) of the electronic/positronic flux densities also applies at TeV energies and since the temperature of the positronic plasma component is lower than of the electrons, cf. Table 1, we predict a broad spectral peak of the positron fraction at around 1 TeV which is followed by exponential decay, see after (5.1) and Fig. 3.

References

[1] AMS Collaboration, Phys. Rev. Lett. 113 (2014) 121102.
[2] J. Casaus, J. Phys.: Conf. Ser. 631 (2015) 012046.
[3] P.D. Serpico, Astropart. Phys. 39 (2012) 2.
[4] O.S. Garania, M.Yu. Romanovsky, Physica A 427 (2015) 1.
[5] A. Montakhab, L. Shahsavar, M. Ghodrat, Physica A 412 (2014) 32.
[6] W. Israel, Physica A 106 (1981) 204.
[7] J.L. Lebowitz, Physica A 194 (1993) 1.
[8] S.R. de Groot, Physica A 88 (1977) 425.
[9] R. Tomaschitz, Physica A 307 (2002) 375.
[10] X.J. Wen, Physica A 392 (2013) 4388.
[11] A.M.S. Kumar, J.P. Prasanth, V.M. Bannur, Physica A 432 (2015) 71.
[12] G.M. Kremer, Physica A 393 (2014) 76.
[13] P.A. Andreev, Physica A 432 (2015) 108.
[14] J.A. de Sales, T. Costa-Soares, V.J. Vasquez Otoya, Physica A 391 (2012) 5422.
[15] R. Yano, K. Suzuki, H. Kuroda, Physica A 381 (2007) 8.
[16] M. Takamoto, S. Inutsuka, Physica A 389 (2010) 4580.
[17] M.H. Duong, Physica A 439 (2015) 34.
[18] HESS Collaboration, Phys. Rev. Lett. 101 (2008) 261104.
[19] AMS Collaboration, Phys. Rev. Lett. 113 (2014) 121101.
[20] N. Volkov, A. Lagutin, A. Tyumentsev, J. Phys.: Conf. Ser. 632 (2015) 012027.
[21] P. Lipari, EPJ Web Conf. 99 (2015) 14001.
[22] X. Li, et al., Phys. Lett. B 749 (2015) 267.
[23] C.-H. Chen, C.-W. Chiang, T. Nomura, Phys. Lett. B 747 (2015) 495.
[24] R. Tomaschitz, Physica A 385 (2007) 558.
[25] R. Tomaschitz, Physica A 387 (2008) 3480.
[26] S. Ichimaru, H. Iyetomi, S. Tanaka, Phys. Rep. 149 (1987) 91.
[27] R. Tomaschitz, Physica B 405 (2010) 1022.
[28] PAMELA Collaboration, Phys. Rev. Lett. 106 (2011) 201101.
[29] PAMELA Collaboration, Phys. Rev. Lett. 111 (2013) 081102.
[30] Fermi-LAT Collaboration, Phys. Rev. Lett. 108 (2012) 011103.
[31] Fermi-LAT Collaboration, Phys. Rev. D 82 (2010) 092004.
[32] HESS Collaboration, Astron. Astrophys. 508 (2009) 561.
[33] R. Tomaschitz, Europhys. Lett. 104 (2013) 19001.
[34] R. Tomaschitz, Physica A 394 (2014) 110.
[35] S. Ichimaru, Rev. Modern Phys. 54 (1982) 1017.
[36] S. Ichimaru, Rev. Mod. Phys. 65 (1993) 255.
[37] R. Tomaschitz, Europhys. Lett. 106 (2014) 39001.
[38] R. Tomaschitz, Phys. Lett. A 378 (2014) 2337.
[39] R. Tomaschitz, Phys. Lett. A 378 (2014) 2915.
[40] R. Tomaschitz, J. High Energy Astrophys. 8 (2015) 10.
[41] A.V. Karelin, et al., J. Phys.: Conf. Ser. 632 (2015) 012014.